Conversion of titanium hydride to titanium nitride during mechanical milling

Heng Zhang and Erich H. Kisi
Department of Mechanical Engineering, The University of Newcastle, Callaghan, New South Wales 2308, Australia
(Received 2 December 1996)

The response of a stable titanium hydride to severe mechanical milling treatments at room temperature was studied in different gaseous environments using different milling media. Structural details were monitored by Reitveld refinements using x-ray-diffraction data and hydrogen compositions were measured by decomposition at 850 °C in a constant volume system. Milling in an argon atmosphere produces only nanocrystalline TiH_x with a reduction in hydrogen content proportional to the milling time. Milling in steel and Co bonded WC vials in air gave a more rapid loss of H and simultaneous formation of TiN. The lattice parameters of both the TiH_x and the Ti formed by decomposition support a mechanism based on solid solution of N in the TiH_x followed by partition into two phases. This resembles a chemically enhanced version of the ''solid-solution pumping'' mechanism previously described for the nitrogenation of pure Ti milled in air. Experiments with different milling media and minor additions of Fe and or Co suggest that 3*d* transition metal is necessary for the nitrogenation to occur, most likely by promoting dissociative chemisorption of N_2. [S0163-1829(97)01121-1]

I. INTRODUCTION

Solid-state phase transitions in intermetallic compounds during high-energy ball milling have generated considerable interest.[1,2] An initially homogeneous intermetallic compound can be transformed to an amorphous state [YCo,[3] NiZr,[4] NiTi,[5] ZrAl,[6] CoZr,[7] NiSn,[8] CoTi,[9] NbSn,[10] CoGe, and GeAl (Ref. 11)]; a solid solution [V_3Ga and Nb_3Au (Refs. 12 and 13)]; or undergo a crystal structure transformation [e.g., Co_3Sn_2 and Ni_3Sn_2 (Refs. 14 and 15)]. In addition, atomic disorder during the early stages of milling has been observed in many ordered compounds with $L1_2$-type structure [Ni_3Al,[16] Ni_3Ge,[6] Ni_3Si (Ref. 17)]; B_2-type structure [AlRu,[18] CoAl,[19] CoGa,[21] and CoZr (Ref. 21)]; $B8$-type structure [Mn_3Sn_2, Fe_3Sn_2,[22,23] Co_3Sn_2, Ni_3Sn_2,[14,15] Co_2Ge,[24] and Co_2Si (Ref. 25)]; and the $A15$ structure [Nb_3Au (Ref. 26) and Nb_3Sn (Ref. 27)]. Investigation of the milling of intermetallic compounds has lead to the synthesis of metastable phases or states with special characteristics unable to be obtained by other methods.

In addition to the above metal-metal or metal-metalloid systems, there is another group of compounds, the metal-gas systems such as oxides, nitrides, and hydrides. While the nitriding of milled pure metals or alloys has been studied, there are no reports of the effects of milling on stable nitrides or hydrides. When compared to intermetallic compounds, these metal-gas compounds have an additional degree of freedom. That is, gas atoms can be desorbed or absorbed during the milling process thereby causing the system to have a variable composition and mass.

In considering oxides, nitrides and hydrides, it should be remembered that often the hydride phase will have the lowest enthalpy of formation. A perfect illustration is the system studied here. Stoichiometric TiH_2 has a formation enthalpy of about -14.96 kJ/mol,[28] whereas TiN and TiO have -336.6 and -542.9 kJ/mol, respectively.[29]

If we take the size of the enthalpy of formation as a first-order indication of the stability of the compound, one expects the hydride to be the least stable. During conventional hydriding, TiH_x can tolerate a wide band of hydrogen concentrations without undergoing structural phase changes from the body-centered tetragonal TiH_2 structure. There is however a temperature-induced transition to the cubic CaF_2 structure at 310 K.[30] All these features lead us to expect a high likelihood that TiH_2 would undergo interesting changes during milling.

II. EXPERIMENTAL

The starting material for these experiments was $TiH_{1.73}$ powder (Research Organic/Inorganic Chemical Corporation, Sun Valley, California 91352) with particle size about 5–8 μm (-325 mesh). The $TiH_{1.73}$ powders were milled in a Shaker mixer/mill (Spex 8000) with an operating cycle of 45 min on and 15 min off. The majority of the ball milling was performed in a hardened steel vial and balls under an air or argon atmosphere. The argon and air atmospheres were obtained by charging the powders into a vial in an argon-filled glove box or just in air, respectively. Approximately 5 g of powder was sealed by an O ring in a vial and the initial weight ratio of balls to powders was 3:1. After different milling times, the vial was opened in a glove box under argon (for an argon atmosphere) or directly in air (for an air atmosphere) and a small amount of powder was taken out for x-ray diffraction (XRD). A similar milling procedure was also carried out in zirconium dioxide and tungsten carbide vial and balls operated in air, in order to identify the effect of the milling media.

A Sieverts-type gas-solid reaction apparatus was used to measure the amount of dehydrogenation induced by milling, and the stability of the milled products. The ultimate vacuum in this system is about 4×10^{-4} Pa and the sensitivity to gas pressure change is 700 Pa. The hydrogen content of the powders was calculated from the pressure rise during heating to 850 °C in an initially evacuated chamber of known volume.

The structure information was monitored by using a Phil-

ips PW1700 x-ray diffractometer (XRD) with Cu $K\alpha$ radiation. Rietveld refinement analysis based on the x-ray-diffraction data was used to assist with phase identification and the refinement of lattice parameters. The microstructure of the milled powders was observed by scanning electron microscopy (SEM) (JOEL JSM-840) with 15-kV accelerating voltage. Powders for SEM examination were mounted in epoxy resin and polished with 1 μm diamond to give a cross-sectional view of agglomerates.

III. RESULTS

The x-ray diffraction patterns at different stages of milling are shown in Fig. 1. Figure 1(a) is for powders milled in argon and Fig. 1(b) for milling in air. Figure 1(a) shows a pattern typical of the original body-centered-tetragonal structure (space group $I4/mmm$) of titanium hydride. The c/a ratio is about 1.3925 [$a_0=3.1596(6)$ and $c_0=4.3996(9)$ Å] based on Rietveld refinement. The lattice parameters for the initial $TiH_{1.73}$ are less than those of the stoichiometric titanium dihydride, $a_0=3.202$ and $c_0=4.279$ Å (Ref. 30) because of the lower hydrogen content. After milling for 5 h, all the diffraction peaks were broadened, and the overlapping of peaks corresponding to (222), (311), (113) planes can be observed. It is no longer immediately clear if the structure is still body-centered-tetragonal, or if it has converted to the high-temperature cubic form (see below and Sec. IV A). Further development of the broadening of all the diffraction peaks can be seen after milling for 15 and 30 h. For the sample milled for 30 h, a set of weak peaks corresponding to a new phase can be distinguished in addition to the peaks corresponding to the titanium hydride. In the light of the results below for milling in air, we believe these peaks resulted from light leakage of air into the vial. The considerable broadening of all the diffraction peaks is primarily due to the refinement of crystallite size with a small contribution from internal stress induced by severe mechanical deformation.

The structural evolution of the titanium hydride milled in air is quite different [Fig. 1(b)]. Again, broadening of all the Bragg diffraction peaks appears after just 5 h milling. The difference occurs when a new set of diffraction peaks at approximately $d=2.12$, 1.50, 1.29, and 1.22 Å become prominent after milling for 15 h. After milling for 30 h, all the peaks from titanium hydride have disappeared, and were replaced by a new phase with the NaCl structure; either titanium nitride or titanium oxide. The new phase keeps the same structure after a further 20 h milling (except for some iron impurity from the milling medium) showing that it possesses good stability [Fig. 1(b)].

Figure 2 shows the crystallite size as a function of milling time. It was estimated using the Scherrer equation and Rietveld refinement[31] results after correction for the instrument profile. It should be noted that when measured in this way, ''crystallite size'' refers to the mean size of coherently diffracting crystal domains and does not indicate how the crystallites are assembled into particles nor how the particles are assembled into agglomerates. The results indicate that the crystallite size for the titanium hydride decreases very quickly during the early stages of milling. After milling for 30 h in argon the crystallite size was reduced to only 45 Å.

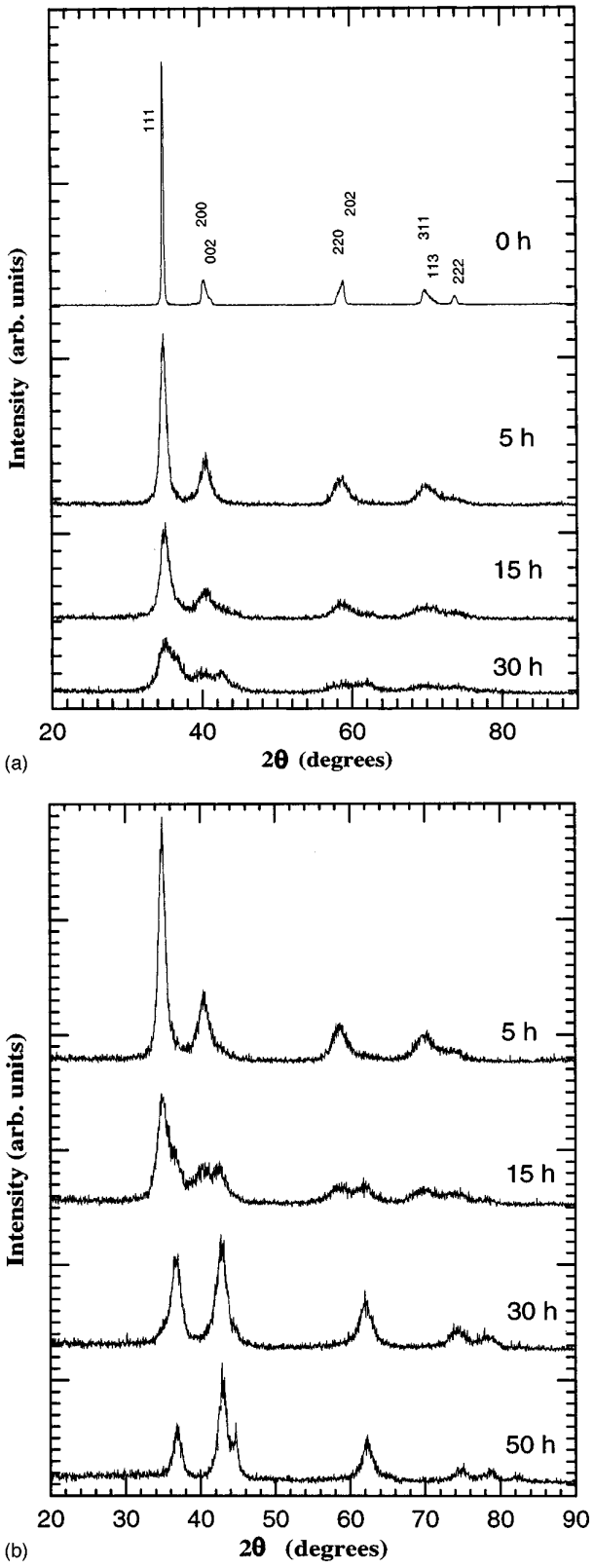

FIG. 1. XRD patterns for $TiH_{1.73}$ milled under argon (a) and air atmosphere (b) vs milling time.

Milling in air has a very similar effect on the particle size of the titanium hydride (Fig. 2) except that the formation of the new phase makes the determination unreliable beyond 15 h. The crystallite size of the new phase increases with further milling even when it comprises 100% of the powder. Be-

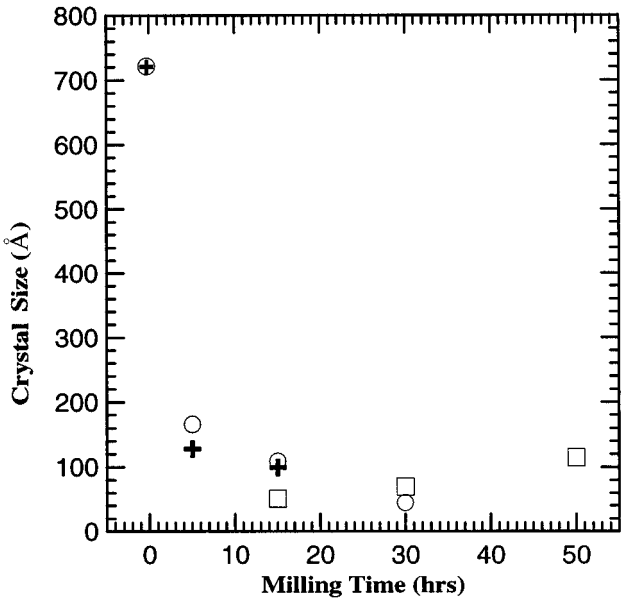

FIG. 2. Crystallite size of titanium hydride milled under argon ○ and air + atmosphere, and the new phase □ vs milling time.

cause our crystallite size measurements refer to coherently scattering (near perfect) domains, we interpret the size increase as indicating recrystallisation of adjoining domains to form larger crystallites of the new phase.

The microstructures generated during milling in the steel vial in air can be seen from the scanning electron microscope (SEM) images presented in Fig. 3. The complicated and heavy deformation during milling causes the hydride powder to be crushed into fine particles. Simultaneously, the fine particles are agglomerated into aggregates of quite large size. These two processes lead to a quite inhomogenous particle size distribution. Fine particles of less than 0.5 μm coexist with agglomerates up to 500 μm. As milling continues, the fraction of very fine particles increases, however, the size of the larger agglomerates also increases. We believe that the milling is quite dynamic with agglomerates fragmenting and reforming continually.

Results for the hydrogen content of the milled powders

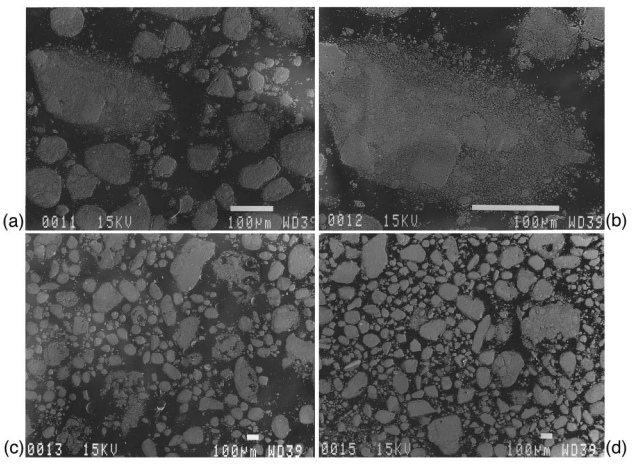

FIG. 3. Microstructure of titanium hydride and the new phase during the milling process (a), (b) 15 h, (c) 30 h, and (d) 50 h.

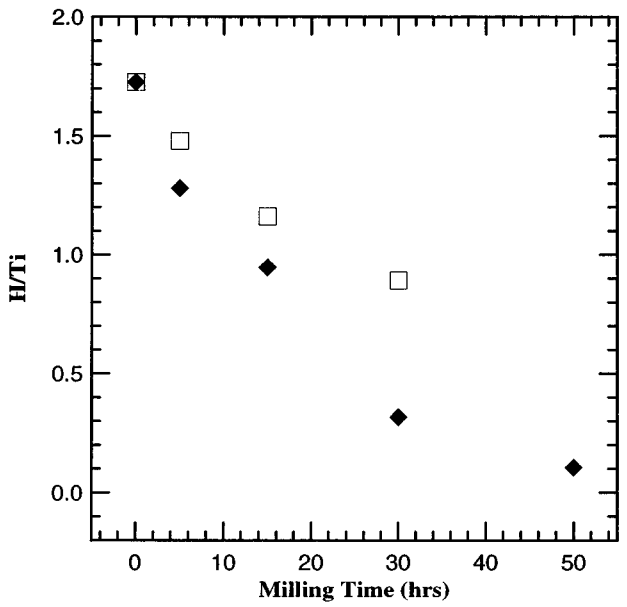

FIG. 4. The atomic ratio of hydrogen to titanium H/Ti as a function of milling time for milling in argon □ and air ◆ measured by decomposition at 850 °C.

(measured by decomposition at 850 °C) are presented in Fig. 4. The structure was tested by XRD after dehydrogenation and the results are shown in Fig. 5. For the case of milling in argon, the residual hydrogen composition TiH_x decreases

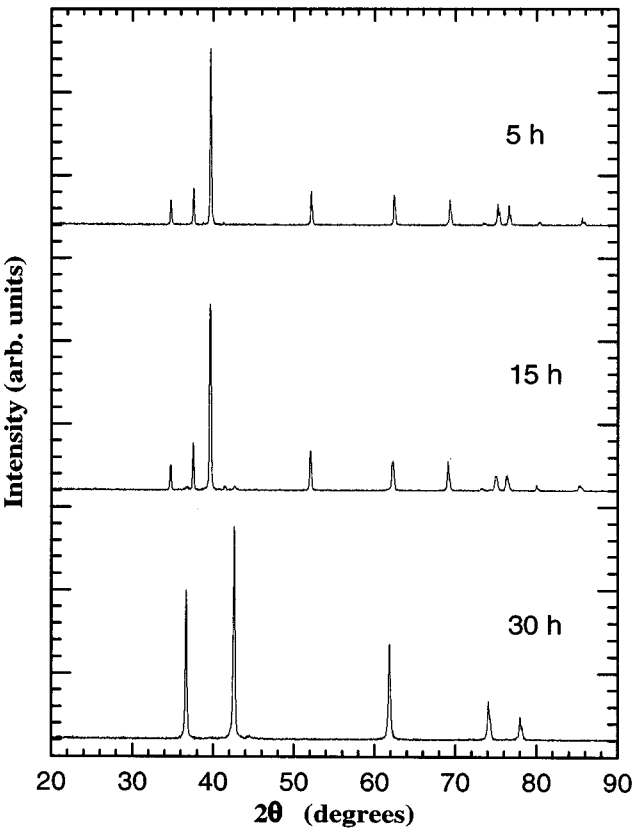

FIG. 5. XRD patterns for the samples dehydrogened at 850 °C after different milling times in air.

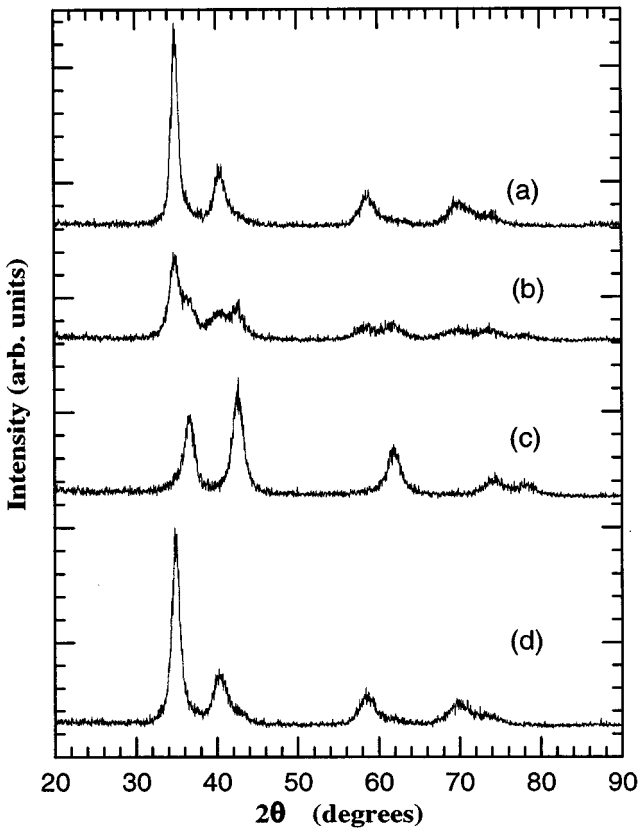

FIG. 6. XRD patterns for $TiH_{1.73}$ milled in a WC vial for (a) 5 h, (b) 15 h, (c) 30 h, and (d) in a ZrO_2 vial for 30 h in air.

from $x=1.73$ initially to $x=1.480$, 1.162, and 0.893 after milling for 5, 15, and 30 h milling, respectively. An interesting phenomenon is that the hydride still appears to display a bct structure although the ratio of H/Ti is only 0.893 (see discussion). For milling in air, the dehydrogenation rate is much faster than that under an argon atmosphere. The ratio of H/Ti decreases to 0.316 and 0.105 after milling 30 and 50 h, respectively. For the latter two samples, there was still residual hydrogen although the sample had transformed to a new phase [Fig. 1(b)].

Examination of the XRD patterns shows that dehydrogenation of the starting material $TiH_{1.73}$ at 850 °C results in pure Ti (hexagonal, $P6_3/mmc$) as expected.[32] Samples milled for 5 to 30 h under an argon atmosphere also show only the titanium XRD pattern after dehydrogenation.

However, the results are quite different for the samples milled in air (see Fig. 5). The sample milled for 5 h shows the titanium structure. After 15 h milling, in addition to the Ti pattern, two weak diffraction peaks are seen at $d=2.12$ and 2.42 Å. These correspond to a new phase with the NaCl structure. For the sample milled for 30 h, only sharp lines corresponding to the new phase with the NaCl crystal structure are visible. The lines have sharpened because of the coarsening of the crystallite size and the elimination of defects. The ability to survive heating to 850 °C in high vacuum provides extra evidence for the stability of the new phase.

Figure 6 presents the XRD patterns for the titanium hydride milled in air with WC and ZrO_2 vials, respectively. The results for milling in the WC vial are very similar to those for the steel vial; all the hydride transformed to a new phase with the NaCl structure after 30 h milling. However, the situation using the ZrO_2 vial is very different, with only broadening of the hydride diffraction peaks observed after 30 h milling. The difference of the structural evolution using the different vials (Fe, WC, and ZrO_2) indicates that the milling medium is a very important factor during the milling of titanium hydride.

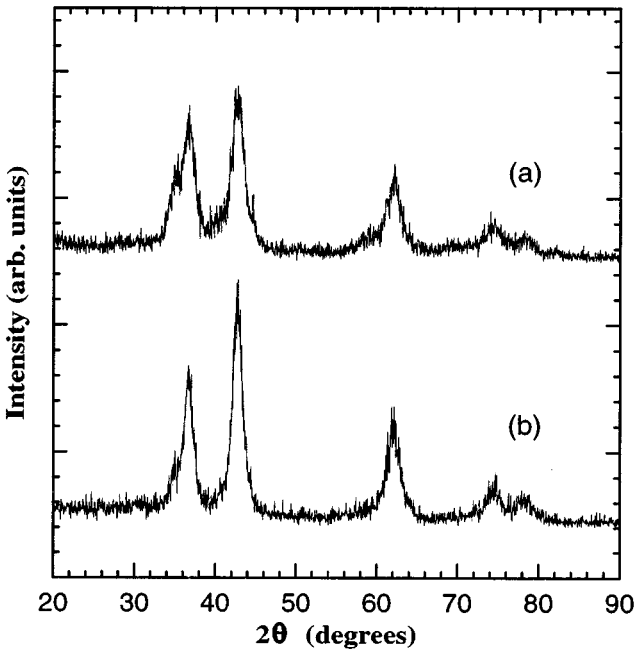

FIG. 7. XRD patterns for the mixture of $(TiH_{1.73})_{98}M_2$ (wt %) [M = Fe for (a), and Co for (b)] milled in a ZrO_2 vial under an air atmosphere.

It was noted that the WC vial material is bonded by cobalt. The presence of a transition metal element (Fe, Co) may play a special role in the transition. Two mixtures of titanium hydride with 2% (wt) iron, or cobalt powder were milled with the ZrO_2 vial under identical experimental conditions as the pure hydride. The results are shown in Fig. 7 and give strong support for the above hypothesis. In both cases most of the hydride transformed to a new phase with the NaCl structure.

IV. DISCUSSION

A. Phase analysis for the milled products

It was apparent in Sec. III that milling under argon causes TiH_x to partially decompose. In addition, the crystallite size is rendered extremely fine. Visual inspection of the diffraction patterns [Fig. 1(a)] is not sufficient to ascertain whether the milled powders have returned to the bct low-temperature form or remained in the high-temperature fcc phase that exists at the average milling temperature ($\sim$323 K). Rietveld analyses based on the fcc model return slightly worse R values than for the bct model. As an example, $R_B=7.85\%$ for the fcc model and $R_B=6.33\%$ for the bct model applied to the XRD data for the sample milled for 30 h in argon. With

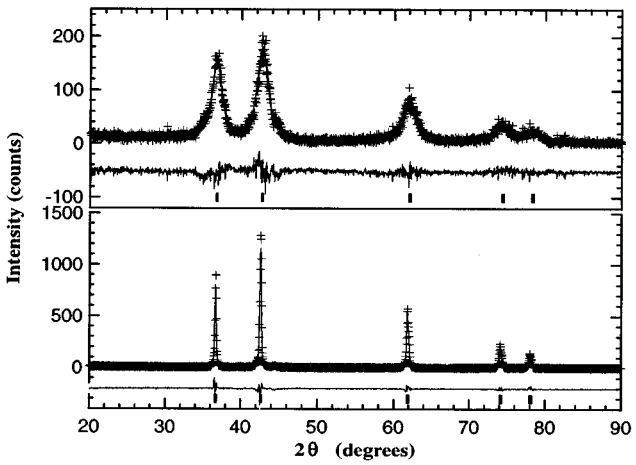

FIG. 8. Rietveld refinement results for samples milled for 30 h in air (a) and subsequently annealed at 850 °C (b). The XRD data are given as + signs and the difference plot and calculated intensities are shown by solid lines.

so few reflections and such broadened peaks, we must regard this improvement as supporting the bct model, but not as conclusive evidence. For example, the Hamilton test[39] applied to these R_B values indicates that we may have about 80% confidence in rejecting the fcc model.

The powders milled in air present a more complex situation. Milling results in decomposition of the hydride and eventual reaction of the milled product with air to form either TiN or TiO. It is not immediately apparent which is formed since their XRD patterns and lattice parameters are similar. Both can be nonstoichiometric with a corresponding range of lattice parameters and the Ti L lines overlap the nitrogen and oxygen K lines in energy-dispersive spectroscopy spectra.

Previous work on pure Ti milled in air[38] provided considerable evidence that the compound formed was TiN, as summarized below:

(i) The lattice parameter of the milled product [4.230(3) Å] is far closer to that of TiN (4.2400 Å),[33] than that of stoichiometric TiO (4.174 Å).[34]

(ii) The effect of nonstoichiometry is to reduce the lattice parameter due to the formation of vacant Ti sites. The lattice parameter of TiO_x may be described as[35]

$$a = 4.23 - 0.05167x,$$

which can clearly not attain a value of 4.230 for nonzero values of x since the minimum oxygen composition for TiO_x can be about 0.536.[36]

(iii) Rietveld analyses based on the XRD data show that
(a) the agreement index R_B is poor and,
(b) unrealistic thermal parameters result when a TiO model is used in the analysis. Further explanation is given in Ref. 37.

(iv) Heating under high vacuum leads to a lattice parameter very close to that of stoichiometric TiN.

(v) Laser Raman spectroscopy and x-ray photoemission spectroscopy also supported these conclusions.

Similar tests (i–iv) were applied to the milled product in these experiments (Fig. 8 and Table I) leading us to conclude that TiN forms in preference to TiO. The increase in lattice parameter after vacuum annealing at 850 °C to 4.2409(3) Å is presumably due to the annihilation of lattice defects such as Ti vacancies. The lattice parameter of TiN_x is known to decrease as x is varied from 1.[39,40]

TABLE I. Results of Rietveld refinements for $TiH_{1.73}$ at milled and annealed states. A: $TiH_{1.73}$ milled 30 h; B: $TiH_{1.73}$ annealed at 850 °C after milled 30 h.

Model	Sample	A	B
TiN	Parameters		
	a (Å)	4.230(3)	4.2409(3)
	B_{Ti}	1.0(1)	0.4(1)
	B_N	3.0(3)	0.2(2)
	r (Å)	70.0	761
	(R_B %)	4.33	3.28
	GOF	1.37	1.59
TiO	Parameters		
B_i fixed	a (Å)	4.232(3)	4.2408(4)
	B_{Ti}	1.0(1)	0.4(2)
	B_N	3.0(3)	0.2(2)
	(R_B %)	9.23	9.15
	GOF	1.56	1.76
TiO	Parameters		
B_i variable	a (Å)	4.228(3)	4.2408(3)
	B_{Ti}	1.22(2)	0.6(1)
	B_N	6.7(4)	2.92(3)
	(R_B %)	6.09	3.29
	GOF	1.43	1.59

B. Milling under argon

The results obtained from milling $TiH_{1.73}$ under argon provide a reference which helps us understand the more complex behavior during milling in air. There are two primary effects here; rapid crystallite size reduction (Fig. 2) and partial dehydriding (Fig. 4). In addition, there are more subtle effects such as a reduction in the unit-cell volume and the c/a ratio. This is summarized in Table II(a). Both are believed to result from loss of hydrogen during the milling process. Titanium hydride is very stable since, under normal circumstances, temperatures exceeding 800 °C are required to cause total decomposition. We take this to indicate either that the milling process is so severe, it causes very localized temperature excursions approaching 800 °C or that the combined mechanical and thermal excitation locally supplies an equivalent amount of energy to the hydride.

C. Hydrogen desorption and nitrogen absorption during milling in air

Before discussing the results obtained by milling $TiH_{1.73}$ in air, we pause to comment briefly on the milling environment. The powder is subjected to repeated ball/vial and ball/ball collisions. As shown by the SEM micrographs, there is coalescence of finer particles into large agglomerates. Simultaneously, the size of the ''perfect'' crystallites is progressively reduced and parts of the material are reacting with nitrogen from the air. It is difficult to form a general model

TABLE II. Unit-cell parameters from the Rietveld Refinement for $TiH_{1.73}$ milled under argon, air atmosphere, and annealed at 850 °C after milling. TiH_{1A}, TiH_{2A}, and TiH_{3A} are $TiH_{1.73}$ milled 5, 15, and 30 h under an argon atmosphere. TiH_0, TiH_1, and TiH_2 are the $TiH_{1.73}$ milled 0, 5, and 15 h in air. $TiH_{0.8}$, TiH_{18}, and TiH_{28} are samples annealed at 850 °C after milling for 0, 5, and 15 h in air. The parameters are based on the bct TiH_2 structure for the milled series and hcp Ti for the annealed series.

Parameter / Sample		a (Å)	c (Å)	c/a	V_{unit} (Å^3)
(a)					
Milled	TiH_{1A}	3.714(3)	4.382(1)	1.3806	44.15
in Ar	TiH_{2A}	3.144(6)	4.324(2)	1.3535	44.13
	TiH_{3A}	3.200(4)	4.198(7)	1.3119	43.00
(b)					
Milled	TiH_0	3.1596(6)	4.3996(9)	1.3925	43.92
in air	TiH_1	3.175(3)	4.366(4)	1.3751	44.01
	TiH_2	3.191(3)	4.356(6)	1.3651	44.35
(c)					
Vacuum	TiH_{08}	2.938(3)	4.707(3)	1.6021	35.19
annealed	TiH_{18}	2.9660(4)	4.7743(4)	1.6099	36.38
	TiH_{28}	2.9738(6)	4.7937(6)	1.6121	36.71

for such a chaotic nonequilibrium environment. However, there is a remarkable degree of homogeneity in the final milled powders which can be revealed by vacuum annealing the powders as outlined below.

It appears that the nitrogenation occurs by three overlapping processes; H desorption, N absorption, and TiN nucleation and growth. Since the milling vial and its contents warms up to approximately 323 K during use, we expect the hydride to quickly transform to the cubic high-temperature form. All subsequent events take place in this form.

It is quite clear from Fig. 4 that there is enhanced desorption of hydrogen when the hydride is milled in the presence of air. We believe this is due to the absorption of N in the early stages of milling. Evidence for nitrogen absorption throughout the milling process comes firstly from an increase in the unit-cell volume, despite the loss of some H. Table II(b) shows this effect and it may be contrasted with the reduction in cell volume that occurs during milling in argon [Table II(a)]. The unit cell of TiN is smaller than that of $TiH_{1.73}$ (in the pseudo-cubic face-centered setting), so only by combined occupancy by H and N may we understand a cell expansion.

During the transition TiH_x to TiN, the tetrahedrally coordinated H is replaced by the octahedrally coordinated N atoms. In this sense, it might be expected that the transition occurs in a smooth fashion across the composition range TiH_xN_y (x from $1.7 \rightarrow 0$, y from $0 \rightarrow 1$). The XRD traces tend to contradict this expectation. In Fig. 1(b), there are definitely two sets of diffraction peaks indicating that there are two populations of crystallites with different average structures, i.e., the solubility limit of N in TiH_x is fairly low before the hydride becomes unstable to TiN.

Further evidence comes from samples milled for 5 and 15 h followed by vacuum annealing at 850 °C [Table II(c)]. We know that such treatment causes removal of all of the H and milling induced effects. Any residual effect on the unit-cell parameters of the resulting Ti is due to absorbed N. From Table II(c) it can be seen that the cell volume of the post heat treatment Ti increases with milling time. After 15 h of milling, there is also a small amount of TiN precipitated (Fig. 5).

The precipitation and growth of TiN is the final stage of the process. After an apparent incubation time of nearly 15 h, it proceeds to completion within a further 15 h (30 h total milling time) and is insensitive to further milling [Fig. 1(b)].

D. The mechanism of dehydrogenation and nitrogenation during milling

Standard reaction mechanisms of anion diffusion through a thick film surface layer are not appropriate to either the low average temperature of the milling environment or the rapid and repeated mechanical deformation of the powders in this process.

The previous section presents evidence for the formation of a solid solution of N in TiH_x as an intermediate step to the nucleation of TiN. This is remarkably similar to observations of the nitrogenation of pure Ti by milling in air.[38] In that case, it was proposed that a ''solid-solution pumping'' mechanism operates. The mechanism may be summarized as proceeding in four steps.

(i) A thermal spike occurs very locally in the region of a collision event. During the temperature spike, N is absorbed into α-Ti (in that case) to form a solid solution, which is retained by the rapid decay of the thermal spike, trapping N in the Ti.

(ii) Successive collisions raise the N content to a level close to the solubility limit.

(iii) TiN nucleates homogenously within the powder particles as the solubility limit is exceeded.

(iv) Because the solubility of N falls as the temperature falls, the solid solution becomes supersaturated each time it ''cools'' after a collision. Excess N diffuses from the solid solution causing growth of the TiN precipitates. In a sense, the solid solution ''pumps'' N into the precipitates.

It would appear that a similar mechanism operates here, with the exception that the starting material is $TiH_{1.73}$ instead of Ti, and the desorption of H has to be incorporated into the model.

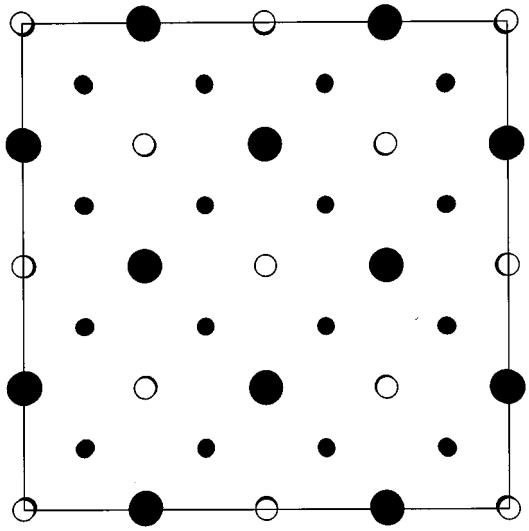

FIG. 9. A [001] projection of the Ti atoms in the TiH_2 structure (with CaF_2 structure) at $z=1/2$: ●, and the coordinating H atoms at $z=1/4$ and $z=3/4$: •. The octahedral sites where interstitial N is absorbed are also shown: ○.

It is clear that milling alone is enough to cause considerable H desorption (Fig. 4), most likely through large, very localized temperature excursions (the hydride is normally relatively stable to $>700\,^{\circ}C$). It is also clear that the absorption of N into TiH_x leads to an enhancement of the H desorption rate. This is quite likely due to a coupling of the thermo/mechanical effects above with chemical and structural effects.

The nitride is for more chemically stable so we expect a large thermodynamic driving force favoring TiN formation. Some insight may be gained from a comparison of the bond strengths, 557.4 kJ/mol (Ref. 42) for Ti—N and 159 kJ/mol (Ref. 41) for Ti═H bonds, respectively.

In addition we must consider the local environment of a N atom absorbed into titanium hydride. Referring to Fig. 9, the Ti atoms form an fcc framework within which the H atoms occupy all of the tetrahedral holes in stoichiometric TiH_2. TiN has the same Ti arrangement, but N occupies the octahedral holes. In the hydride (TiH_2) the octahedral void has a radius (defined by near-neighbor Ti atoms) of approximately 0.76 Å compared with a nominal radius of 0.75 Å for N.

The H atoms in TiH_2 each have four nearest-neighbor (NN) Ti atoms along $1/4\langle 111\rangle$, six next-nearest-neighbor (NNN) H atoms along $1/2\langle 100\rangle$, 12 third-NN H atoms along $1/2\langle 110\rangle$, and eight fifth-NN H atoms along $1/2\langle 111\rangle$ as largely unobstructed neighbors (the fourth-NN are partially screened Ti atoms along $1/4\langle 311\rangle$). The solution of a N atom into TiH_2 therefore requires N to occupy a site with six NNN Ti atoms in an octahedral coordination shell and eight NN H atoms along $1/4\langle 111\rangle$ (between atom centers although the Ti atom is much larger and will exert the greater influence).

The Ti—N bond is largely covalent so firstly we expect a large local perturbation to the charge distribution of the Ti atoms in the vicinity of a N atom. Secondly, the H atoms now have their third NN and fifth NN H-H interactions locally screened by the N atom. The third effect of a N atom in TiH_2 is the direct N-H interaction since they are now in close NNN positions. The N assisted dehydrogenation is likely to have been assisted by (i) the starting material being nonstoichiometric and (ii) initial H loss during the very early stages of milling.

The net effect is to promote more rapid decomposition of the hydride. It should be noted that the rate of TiN formation is very similar to that for pure Ti milled in air, and is probably limited more by the supply of N_2 reaction gas than internal gas-metal reaction processes.

In previous work on the milling of Ti,[38] it was noted that the presence of Fe in the milling vial and balls was necessary to the formation of TiN. No TiN was observed in powders milled in a ZrO_2 vial until a small amount of Fe powder was introduced into the milling charge.

These observations have been reinforced here. $TiH_{1.73}$ milled in air yielded only nanocrystalline TiH_x (Fig. 6) when a ZrO_2 vial was used. However in a Co bonded WC vial, again the product was TiN.

However, $TiH_{1.73}$ mixed with 2 wt. % of Fe or Co and milled in the ZrO_2 vial yields TiN (Fig. 7). We conclude that the presence of minor quantities of a group VIII transition metal is necessary for the nitrogenation to proceed. In previous work[38] we speculated that this may be due either to catalysis of dissociative chemisorption of N_2 on the Fe or Co during collisions. An alternative suggestion is that the transition metals serve as O sinks which reduce the oxygen partial pressure, making nitrogenation the favored reaction.

V. CONCLUSIONS

Ball milling of titanium hydride under an argon atmosphere induces progressive dehydrogenation. Nanocrystalline $TiH_{0.89}$ was obtained after 30 h milling, while milling in air causes simultaneous dehydrogenation and nitrogenation of the titanium hydride. After 30 h of milling, nearly stoichiometric TiN with the NaCl crystal structure and good stability was produced.

The nitrogenation process in titanium hydride is quite similar to that for pure Ti milled in air, but completely different from traditional gas-solid reaction processes. A mechanical-chemical nitrogenation mechanism was proposed to explain the unusual dehydrogenation and nitrogenation induced by ball milling. Formation of a saturated-solid solution of nitrogen by ''pumping'' plays a critical part in nucleation and growth of the nitride during the nitrogenation process. This work further confirms that $3d$ transition metals, Fe and Co from the milling medium appear to play an important role in the nitrogenation process.

[1] C. C. Koch, Mater. Trans. JIM. **36**, 85 (1995).
[2] A. W. Weeber and H. Bakker, Physica B **153**, 93 (1988).
[3] A. Y. Yemakov, Y. Y. Yurchikov, and V. A. Barinov, Fiz. Met. Metallovd. **52**, 1184 (1981).
[4] R. B. Schwarz and C. C. Koch, Appl. Phys. Lett. **49**, 146 (1986).
[5] D. L. Beke, H. Bakker, and P. I. Loeff, J. Phys. **14**, c4-63 (1990).
[6] T. Benameur and A. R. Yavarari, J. Mater. Res. **7**, 2971 (1992).
[7] A. Mehrtens, G. Von Minnigerode, and K. Samwer, Z. Phys. B **83**, 55 (1991).
[8] T. T. Tiainen and R. B. Schwarz, J. Less-Common Met. **140**, 99 (1988).
[9] Y. Seki and W. L. Johnson, in *Solid State Powder Processing*, edited by A. H. Clayer and J. J. de Barbasillo (TMS, Warrendale, PA, 1990), p. 287.
[10] Y. S. Cho and C. C. Koch, Mater. Sci. Eng. A **141**, 139 (1991).
[11] G. F. Zhou and H. Bakker, Phys. Rev. Lett. **72**, 2290; **73**, 344 (1994).
[12] L. M. Di and H. Bakker, J. Phys. Condens. Matter **3**, 3427 (1991).
[13] H. Bakker and G. F. Zhou, Mater. Sci. Forum **88-90**, 27 (1992).
[14] L. M. Di, G. F. Zhou, and H. Bakker, Phys. Rev. B **47**, 4890 (1993).
[15] G. F. Zhou, L. M. Di, and H. Bakker, J. Appl. Phys. **73**, 1521 (1993).
[16] J. S. C. Jang and C. C. Koch, J. Mater. Res. **5**, 498 (1990).
[17] Y. S. Cho and C. C. Koch, J. Alloys Compds. **194**, 287 (1993).
[18] E. Hellstern, H. J. Feeht, Z. Fu, and W. L. Johnson, J. Appl. Phys. **65**, 305 (1988).
[19] L. M. Di, H. Bakker, and F. R. de Boer, Physica B **182**, 91 (1992).
[20] L. M. Di and H. Bakker, and T. Tamminga, Phys. Rev. B **44**, 2444 (1991).
[21] G. F. Zhou and H. Bakker, Physica B **211**, 134 (1995).
[22] G. F. Zhou and H. Bakker, Phys. Rev. B **48**, 7672 (1993).
[23] G. F. Zhou and H. Bakker, Phys. Rev. B **49**, 12 507 (1994).
[24] G. F. Zhou and H. Bakker, Phys. Rev. B **48**, 13 383 (1993).
[25] G. F. Zhou and H. Bakker, J. Phys. Condens. Matter **6**, 4043 (1994).
[26] L. M. Di and H. Bakker, J. Appl. Phys. **71**, 5650 (1992).
[27] L. M. Di, P. I. Loeff, and H. Bakker, J. Less-Common Met. **168**, 183 (1991).
[28] T. R. P. Gibb, Jr J. J. Mscharry, and R. W. Bragdon, J. Amer. Chem. Soc. **73**, 17051 (1951).
[29] Eric A. Brandes, *Smithells Metals Reference Book*, 6th ed. (Butterworths, London, 1986), pp. 8-24, 8-27.
[30] H. L. Yakel, Acta Crystallogr. **11**, 46 (1958).
[31] R. J. Hill and C. J. Howard (unpublished).
[32] A. D. McQuilan, Proc. R. Soc. London **204**, 309 (1951).
[33] P. Duwez and F. Odell, J. Electrochem. Soc. **97**, 299 (1950).
[34] H. Krainer, Arch Eisenhüettenwes. **21**, 119 (1951).
[35] M. D. Banus, T. B. Reed, and A. J. Strauss, Phys. Rev. B **5**, 2775 (1972).
[36] A. N. Cristensen, Acta Chem. Scand. A **32**, 89 (1978).
[37] W. C. Hamilton, Acta Crystallogr. **18**, 502 (1965).
[38] H. Zhang and E. H. Kisi, J. Phys. D **29**, 1367 (1996).
[39] P. Ehrich, Z. Anorg. Chem. **259**, 1 (1949).
[40] A. Brager, Acta Physicochem. CRSS **11**, 617 (1939).
[41] R. M. Haag and F. J. Shipko, J. Amer. Chem. Soc. **78**, 5155 (1956).
[42] R. J. Wasilewski and G. L. Kell, J. Inst. Met. **83**, 94 (1954/1955).